




Research Article

Analysis of Optimal Load Management Using a Stand-Alone Hybrid AC/DC Microgrid System

Vasantharaj Subramanian ¹, Indragandhi Vairavasundaram ²
and Belqasem Aljafari ³

¹Kings College of Engineering, Pudukkottai 613303, India

²School of Electrical Engineering, Vellore Institute of Technology, Vellore 632014, India

³Department of Electrical Engineering, Najran University, Najran 11001, Saudi Arabia

Correspondence should be addressed to Indragandhi Vairavasundaram; indragandhi.v@vit.ac.in

Received 22 July 2022; Revised 17 November 2022; Accepted 4 April 2023; Published 19 April 2023

Academic Editor: Baseem Khan

Copyright © 2023 Vasantharaj Subramanian et al. This is an open access article distributed under the Creative Commons Attribution License, which permits unrestricted use, distribution, and reproduction in any medium, provided the original work is properly cited.

Typically, diesel or other fossil fuel-based related applications meet electricity demand. Nonetheless, as the cost of fossil fuels rises, as do their harmful emissions, there is a sudden transition toward stand-alone hybrid renewable energy systems (HRESs). The proposed project proposes electrifying VIT University in Vellore, Tamil Nadu, India, using an off-grid HRES. The goal of enhancing hybrid energy system (HES) regulation, size, and component selection is to provide society with a cost-effective power supply. This article's primary purpose is to show how to utilize HOMER Pro Software to reduce total net present cost, cost of energy, and CO₂ emissions. After that, the findings were compared to four different HRES configurations. The efficient solution for transmitting power at the lowest energy cost is configuration 1 (solar + fuel cell + battery + wind + diesel generator) which is found to be the optimal solution for supplying energy with 0% unmet load at the least cost of energy, which is at 24.91 Rs/kWh. These data are used to calculate the optimal size of energy storage components based on long-term system behavior using HOMER and to forecast short-term generation and demand changes while maintaining system dependability and grid voltage. Using and incorporating model predictive control (MPC) for an interlinking converter (ILC), the proposed HRES design is validated for the study area in a novel way that sequentially applies HOMER and MATLAB simulations.

1. Introduction

Wind, fuel cells, biogas, and biomass are sustainable, ecologically friendly, and renewable resources that can be used to create an economy that is more energy efficient. Yet, renewable resources are subject to a wide range of limitations when utilized in a stand-alone, flexible structure. Solar and wind energy resources are combined with other sources to create an HRES to address these issues. As a result, using their benefits makes it feasible to produce energy more efficiently [1–3]. Numerous techniques have been suggested to restore energy balance in microgrid (MG) due to the constraints of the usage of renewable energy sources (RESs) [4]. RESs are integrated with energy storage to solve the issues produced by energy imbalances. Demand response management has been achieved by using software that

optimizes demand-side resources, in addition to recent advancements in smart grid (SG) technology.

Programs for energy management have taken into account residential loads, which make up the majority of the electricity demand [5]. The physical attributes of the structure, such as its location, architecture, and construction, affect how much energy is used at home [6]. Two broad categories can be found in the recent articles regarding the orbit of power plants [7, 8].

- (i) The first category includes the involvement and production plans of power plants to meet the anticipated load and includes a specific amount of reservations or load response plans to account for consumption or production uncertainties in wind power sources.

- (ii) The second category of articles relates to establishing effective random optimization techniques for the program's unit placement.

Hybridized energy can be evaluated using a variety of software packages, the most well-known of which is the National Renewable Energy Laboratory's Hybrid Optimization Model for Electric Renewables (HOMER) [9]. HOMER is just a simulation software program that includes an economic analyzer for evaluating and optimizing a system's economic feasibility. However, in the hybrid system, the software's ability to simulate the system at a high level to test alternative control techniques or rapid load adjustments to study instantaneous system behavior is limited. In works like [10, 11], linear programming methodologies within MATLAB were used to build microgrid (MG) models and examine their findings in contrast to dynamic performance, necessitating mathematically derived models of every element within the network. Numerous analyses utilized HOMER to size, optimize, and study the effectiveness of the complete system while using Simulink to operate the device [12], execute a load flow analysis [13], or investigate the dynamic nature of the system's various sources [14]. Different configurations of HESs were developed with four configurations, and the economic feasibility solution can be determined using HOMER software. Of the four configurations, configuration 1 is the most economically viable option with a COE of 24.91 Rs/kWh.

The usage of MPC is justified by the fact that this algorithm is generally regarded as one of the most potent nonlinear programming and artificial intelligence techniques. MPC is well suited to solve the problems of power systems and power plants because of its advantages in handling the systematic processing of restricted multivariable [15]. By predicting future control actions, hierarchical and distributed MPC is more effective at addressing significant and complex power system issues. Due to its ease of use and excellent accuracy, finite control set MPC (FCS-MPC) is the most popular MPC control [16]. MPC has several benefits in electrical drives, including speed, position, torque control, torque ripple reduction, and field-oriented control [17]. It is also used in load frequency control to increase dynamic response under various disturbances. The proposed FCS-MPC is preferred to the other control techniques in the following ways: (1) it is simple to adjust the control parameters; (2) it can conduct multiobjective optimization and take constraints into account; (3) the decoupling procedure is not necessary; and (4) PWM modulators are not needed [18].

On the other hand, this research does not collect information from off-grid villages obtained through sociological analysis with low-level simulation and complete system optimization. The following are the paper's most important contributions:

- (i) In remote locations, a novel HRES was built for size and cost minimization considerations.

- (ii) The system's stability was confirmed by comparing it to four different stand-alone HRESs with the least NPC and COE values.
- (iii) A network that combines PV, wind, FC, diesel generator (DG), and batteries is efficient.
- (iv) With COE and NPC, sensitivity analysis will be carried out for variations in yearly wind speed and DG fuel price.
- (v) The proposed model significantly benefits the environment, has a short payback period, and produces fewer emissions.

The structure of the study is broken down as follows. Section 2 goes through the hybrid AC/DC MG system in detail, while Section 3 deals with the case study site of the research. Section 4 is intended to have a detailed description of techno-economic analysis utilizing HOMER, along with the ideal design purpose and restrictions supported by a complete flowchart. Section 5 explains the HOMER software-based optimization, and Section 6 discusses the results obtained. Section 7 gives an overview of the future research direction and open issues in the hybrid AC/DC MGs. The conclusion of the research is depicted in Section 8.

2. Overview of Microgrid System

A specific hybrid AC/DC MG is depicted in Figure 1. Four-quadrant three-phase AC/DC converters and transformers connect DC and AC distribution networks. DC/DC boost converters integrate DC power generators to DC networks, such as PV panels and FC stacks. DC loads such as speed control motors and electric automobiles were coupled to the DC grid via DC/DC buck converters. Bidirectional DC/DC converters, like supercapacitors and batteries, integrate DC energy storage devices to the DC grid. A transformer connects the hybrid grid's three-phase AC network, an operational low-voltage distribution network, to the utility grid. Transformers connect AC power generators to the AC grid, such as WTGs and DGs. AC motors and other AC loads are connected to AC networks. The AC grid voltage is either 200 or 400 volts. For the DC grid, there are no typical voltage values. Several testing methods now use voltage levels ranging from 12 V to over 1000 V, depending on the converter and system needs.

3. Case Study Site: Vellore Institute of Technology (VIT), Vellore, India

3.1. Site Information. The hybrid AC/DC MG system proposed in Section 3 is demonstrated using a fieldwork example. The chosen site is VIT University in Vellore, India, as indicated in Figure 2. Because a university campus has its own distributed energy resources (DERs) that may be designed to function as an MG to optimize and enhance energy consumption, this location was selected as a case study. Numerous universities have been researching smart MGs on their campuses and using them as a testbed to investigate the implementation, verification, and validation of innovative concepts and technologies due to their

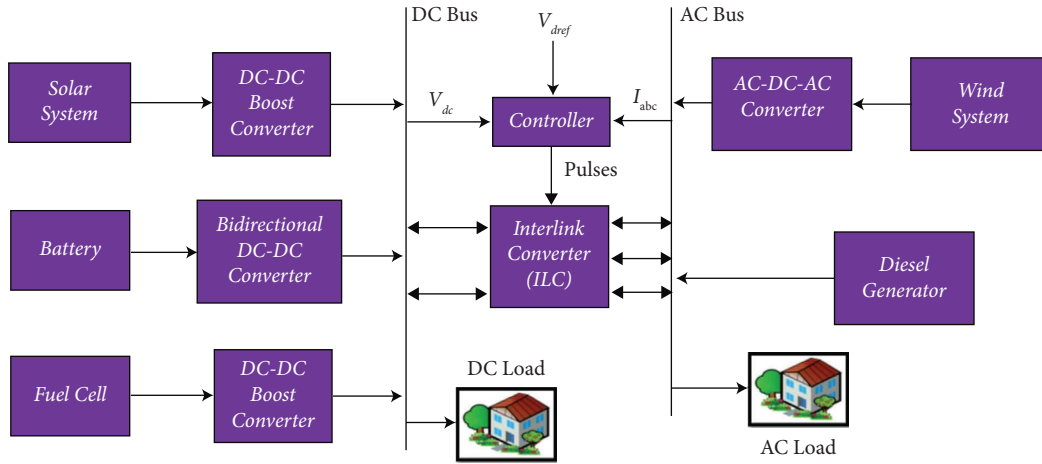


FIGURE 1: Hybrid AC/DC MG system.

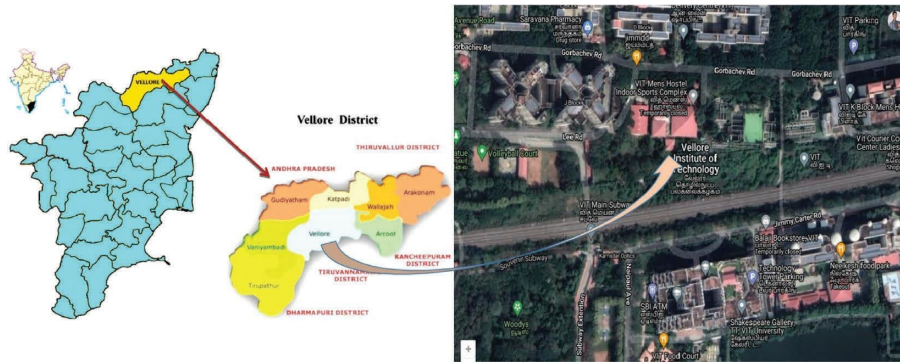


FIGURE 2: Site map of VIT, Vellore.

multiple benefits. The community's goal is to produce its electricity domestically using renewable sources, allowing them to manage system costs and avoid relying on the interrupted fuel supply chain. The field research evaluated present and potential off-grid supply sources and provided background info to aid in determining future demand and MG construction needs in this area.

3.2. Demand Modelling during 24 h Period. The field study has reported analyses of daily municipal energy usage which is shown in Figure 3. The instantaneous power consumption over the course of a day will be unpredictable over the span of a day.

3.3. PV Power Modelling. The mechanism for modelling solar panels was adapted from [19–22]. NASA's daily averaged solar data are combined with GPS coordinates from the site. The location delivers a mean insolation energy of 5.29 kWh/m²/day for a year, rising to 6.730 kWh/m²/day in April. It is then fed into solar panel models, which are then analyzed daily. The temperature impacts PV panel efficiency, so it is accounted for in the solar panel model. Because no local temperature data are available, an average temperature depending on the area was utilized. In-built NASA models have obtained the PV input values for HOMER modelling

based on Vellore's site and altitude, as indicated in Figure 4. Total energy generated by PV (EPV) is stated as

$$E_{PV}(t) = \frac{N_{PV} \times V_{PV}(t) \times I_{PV}(t) \times \Delta t}{1000}, \quad (1)$$

where N_{PV} = no. of PV modules; $V_{PV}(t)$ = PV module voltage; $I_{PV}(t)$ = PV module current; and Δt = step time.

3.4. Wind Power Modelling. During a 6-month duration at VIT, wind data were collected every 10 minutes and then averaged once 2 hours. The averaged wind speed data are coupled with blast modelling, which uses a tiny Gaussian distribution value output with an average of 0 m/s and a variance of 6 m/s to estimate the wind speed. Instead of designing a unique manufacturer's wind turbine (WT), a generic WT model was used to represent the 10 kW WTs expected to be installed in the future. 10 kW WT models are considered under HOMER's optimization parameters. As in HOMER modelling, monthly average wind data are employed. As shown in Figure 5, the wind speed data collected for HOMER modelling relied on in-built NASA models depending on Vellore's site and altitude. Equation (2) expresses the total energy produced by the WT system (E_{WT}) [23]:

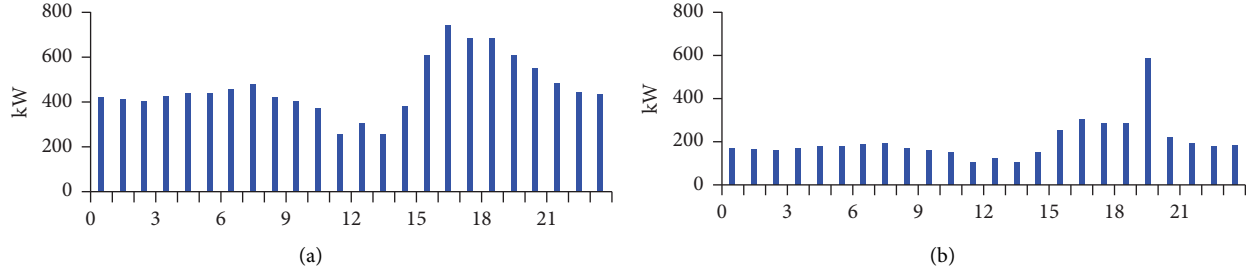


FIGURE 3: Hourly load profile of (a) AC load and (b) DC load.

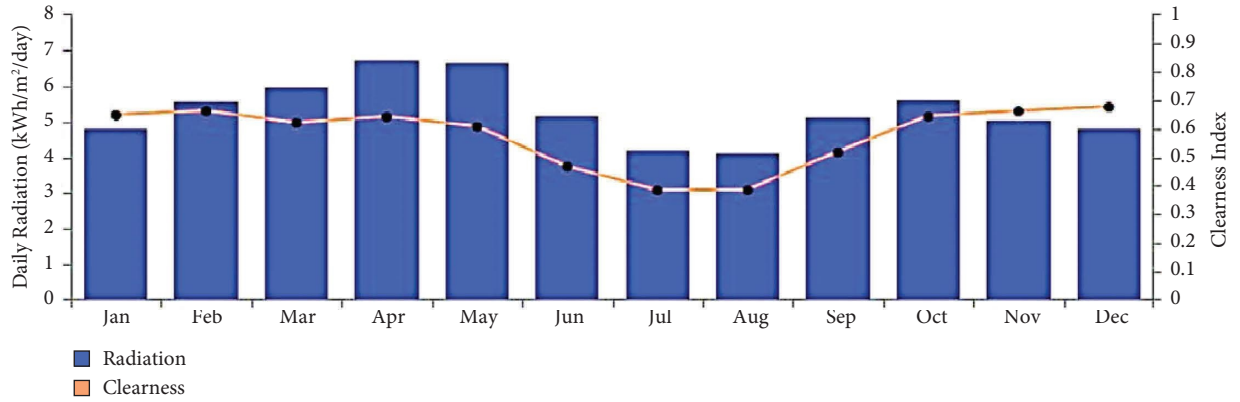


FIGURE 4: Daily averaged solar data.

$$E_{WT}(t) = \frac{N_{WT} \times P_{WT}(t) \times \Delta t}{1000}, \quad (2)$$

where N_{WT} =no. of WT and $P_{WT}(t)$ =WT power.

3.5. Fuel Cell Modelling in HOMER. Like all RESs, the FC system is a viable option, especially on standby in remote applications. Such devices are extremely clean; no emissions are produced, and they are quite efficient. FC provides affordable, scalable, and extremely dependable energy, which is clean, enclosed, modular, quiet, and friendly to the environment. Hydrogen is the principal fuel employed in FC systems, which transforms the stored energy of fuel instantaneously into electricity using an oxidant like methane, ethanol, biomass-based fuels, and so on, based on the type of FC system. Proton exchange membrane (PEM) FCs, among several FC systems, are employed in industrial and commercial applications and have a quick dynamic response time of 1–3 seconds [24]. It performs well even when the supply is imbalanced. FCs of this type is used to generate

significant amounts of electricity. Equation (3) was used to calculate the output power of an FC [25].

$$P_{FC} = P_{tank-FC} \times \eta_{FC}. \quad (3)$$

3.5.1. Hydrogen Tank/Electrolyzer. The electrolyzer operates using the electrolysis process, in which electricity passes from one electrode to other through water and decays into oxygen and hydrogen. In most studies, the electrolyzer output is perfectly matched to the hydrogen storage tank [26, 27]. Equation (4) is used to calculate the amount of power delivered from the electrolyzer to the hydrogen storage tank ($P_{Elec-tank}$).

$$P_{Elec-tank} = P_{ren-elec} \times \eta_{elec}, \quad (4)$$

where $P_{Elec-tank}$ =electrolyzer power output and η_{elec} =electrolyzer efficiency.

Equation (5) expresses the output energy stored by a hydrogen tank.

$$E_{H2-tank}(t) = E_{H2-tank}(t-1) + \left[P_{Elec-tank}(t) - \left(\frac{P_{tank-FC}(t)}{\eta_{storage}} \right) \right] \times \Delta t, \quad (5)$$

where $P_{tank-FC}$ =FC output power and $\eta_{storage}$ =hydrogen efficiency.

3.6. Modelling of Load in HOMER. In HOMER, two different loads were modelled: an AC load and a DC load. In HOMER,

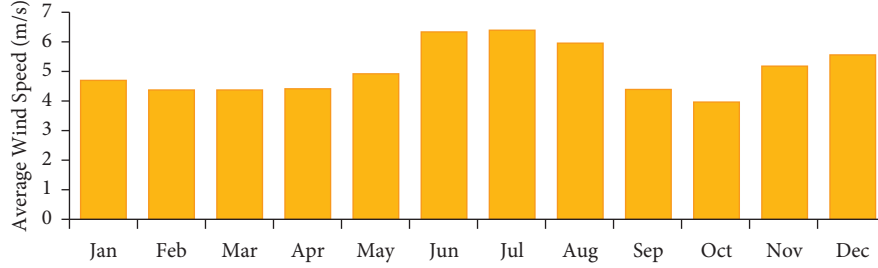


FIGURE 5: Average monthly wind inputs.

the AC load has been estimated hourly, which is depicted in Figure 3(a) as a bar graph. Likewise, a bar graph is given in Figure 3(b) for DC load. Throughout the year, the combined DC load and AC load are constant.

3.7. Storage Modelling in HOMER. The amount of energy produced and consumed depends on the number of batteries connected and the state of each battery at any time. Power generation surpasses load demand when the battery is charged. Strings of 3,201 numbers of 1 kWh have been chosen to give the appropriate bus voltage for HOMER modelling. These batteries have a capacity of 3,201 numbers of 1 kWh each, providing 32,036 kWh of energy storage in the string.

4. FCS-MPC for Interlinking Converter

FCS-MPC is recommended to control DC-AC ILC to regulate the magnitude of the load voltage. This study analyzes FCS-MPC for two-level three-leg voltage source inverters (VSIs). Out of the seven conceivable switching states, the control strategy described chooses the best state to minimize the cost function. Simulation tests of the MPC-based control strategy reveal that output voltage continuously follows the reference value while compensating for load, source, and filter changes without impairing normal inverter functioning. The following section covers specific control and management strategies in detail.

The MPC control scheme's principle is depicted in Figure 6. V represents the variables required to handle and solve a particular situation. The number d symbolizes the disturbance. The control variable is denoted by the letter c . w represents the processed variable's predicted value. The optimizer can be simulated using measurements of the current system (v) and disturbances/forecast values (d). The interlinking voltage source inverter's primary control, including power droop regulation, the reference generator (three-phase), and the inner control loop, is carried out using the FCS-MPC scheme. Unlike conventional controllers, FCS-MPC does not require PI controllers to execute the inner current and outer voltage control loops or other complicated modulation steps (such as PWM and SVPWM), and it has a faster dynamic response than standard control schemes. The following sections discuss the FCS-MPC control mechanism's operating theory.

The inputs for the inner loop, voltage signals from abc to α - β reference, are converted using the Clarke transformation

in the first step. The switching signals for interlinking the VSI are produced using the measurement of the RLC filter. The instantaneous powers (P and Q) and fundamental powers are then estimated using the measurements of RLC filters obtained from primary control. For managing the AC bus voltage, a droop control method using P - V and Q - V is used. Utilizing a three-phase sinusoidal generator to regulate the voltage, the final reference signals for VSI transistors (MOSFETs) are produced. Discrete-time state space (DSS) model is developed. The MPC algorithm predicts voltage vectors for each conceivable combination for the upcoming sample time. The objective functions, input voltage vector, and CSS and DSS models are expressed in [28]. The best voltage vector and its accompanying signals for the IGBT switches of VSI are tested over seven switching states.

The filter model shown in Figure 7 for the predictive voltage control of Figure 8 is

$$\frac{d}{dt} \begin{bmatrix} i_f \\ v_c \\ i_o \end{bmatrix} = \begin{bmatrix} 0 & \frac{1}{L} & 0 \\ \frac{1}{C} & 0 & -\frac{1}{C} \\ 0 & 0 & 0 \end{bmatrix} \begin{bmatrix} i_f \\ v_c \\ i_o \end{bmatrix} + \begin{bmatrix} \frac{1}{L} \\ 0 \\ 0 \end{bmatrix} v_i + \begin{bmatrix} 0 \\ 0 \\ f(i_o, v_c) \end{bmatrix}, \quad (6)$$

where v_c , v_i , i_o , i_f , r_f , and L are load side voltage vector, output voltage of inverter, output current of inverter, filter current, filter resistance, and inductance. CSS model can be expressed as

$$\frac{dx}{dt} = Ax + Bv_i + u_d(k). \quad (7)$$

DSS modelling is used to predict voltage as

$$x(k+1) = A_q x(k) + B_q v_i(k) + u_d(k). \quad (8)$$

By using the DSS model, we determine,

$$\begin{bmatrix} V_c \\ I_f \end{bmatrix}^{k+1} = A_d \begin{bmatrix} V_c \\ I_f \end{bmatrix}^k + B_d \begin{bmatrix} V_i \\ I_o \end{bmatrix}, \quad (9)$$

where $A_q = e^{AT_s}$, $B_q = \int_0^{T_s} e^{A\tau} B d\tau$, and V_i is input voltage vector with seven possible switching states for VSI switches (S_a , S_b , S_c):

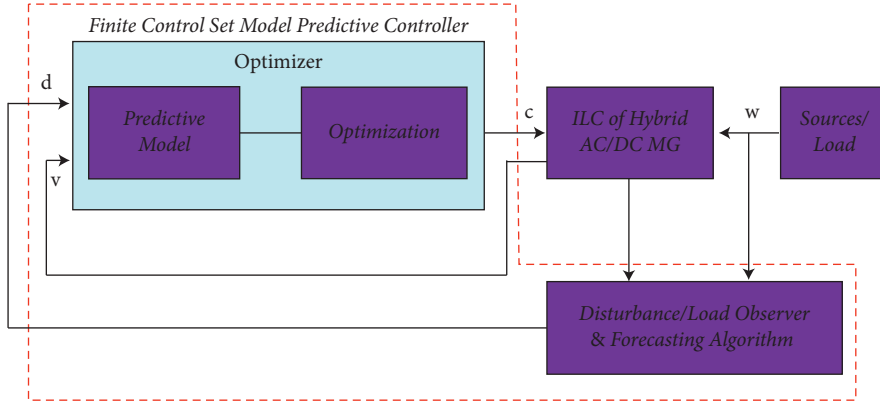


FIGURE 6: Applied FCS-MPC control for an ILC of HMG.

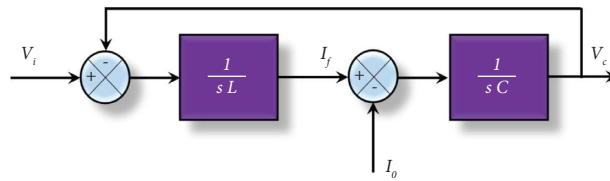


FIGURE 7: Filter model for predictive voltage control.

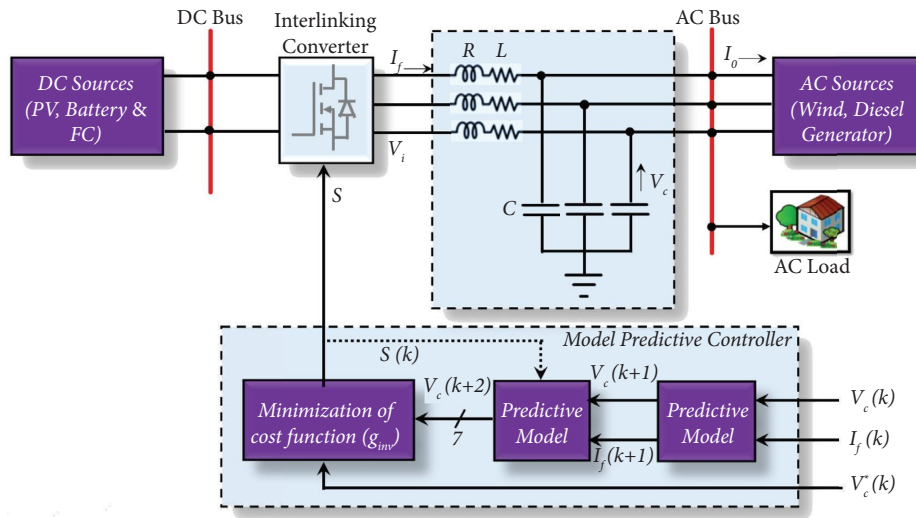


FIGURE 8: FCS-MPC scheme for interlinking converter.

$$V_n = \begin{cases} \frac{2}{3}V_{dc}e^{j(n-1)\pi/3}, & \text{for } n = 1, 2, \dots, 6, \\ 0, & \text{for } n = 0, 7. \end{cases} \quad (10)$$

The following cost function is suggested for the load observer:

$$g_{inv} = (v_{ca}^* - v_{ca})^2 + (v_{cb}^* - v_{cb})^2. \quad (11)$$

The implemented algorithm's flowchart for inverter control in islanded mode is shown in Figure 9. The inverter output voltage magnitude regulates the active power, and the

inverter frequency regulates the reactive power. In an AC microgrid, power flow (active and reactive) across distributed energy resources (DERs) is controlled using voltage amplitude (V_{nom}) and angular frequency (ω_{nom}) of the inverter output voltage as specified in expressions (12) and (13).

$$\omega_i = \omega_{nom} - m_i P_i, \quad (12)$$

$$V_i = V_{nom} - n_i Q_i. \quad (13)$$

The coefficients (m and n) are selected based on the following relations to ensure system stability.

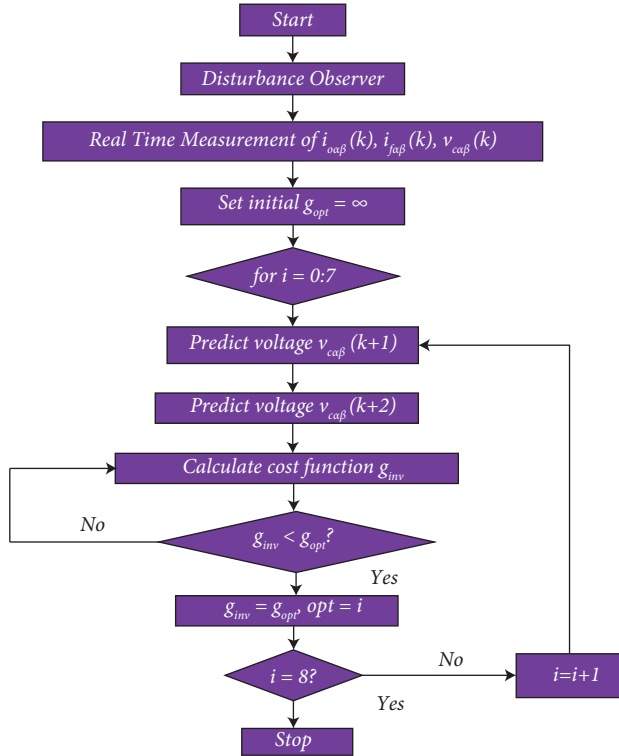


FIGURE 9: The flowchart of the implemented FCS-MPC algorithm.

$$m_i = \frac{\Delta\omega}{Q_{\max}}, \quad (14)$$

$$n_i = \frac{\Delta V}{P_{\max}},$$

where P_{\max} and Q_{\max} are the maximum powers supplied by the inverter and $\Delta\omega$ and ΔV are maximum deviations of frequency and voltage amplitude of the inverter output.

5. Optimization of MG Using HOMER Software

5.1. HOMER Pro Software Helps with Optimization. A reliable techno-economic optimization program called HOMER [29] enables the analysis and simulation of techno-economic models and the design optimization of HRES units. With the help of its optimization algorithms, the developer and decision makers can determine alternative technical solutions and economic viability while considering changes in technology costs and available resources. To find the best model to meet the load demand of the specified location, HOMER is considered for techno-economic analysis.

HOMER analyzes numerous possibilities quickly and readily in search of viable and desirable alternatives. The sizes of PV panels, the quantity of WTs, the amount of battery storage, and the number of converters are all optimized using HOMER [30]. The objective function of the HOMER optimization strategy is total NPC, which is based on input parameters such as load demand, energy resource data, economic and technical aspects of each component,

design constraints, proposed management, and control strategy, emission data, and design constraints. The technical, environmental, and economic aspects of HRES are evaluated using HOMER analysis based on one-year optimization [31]. Following that, all expenditures are extrapolated over the remaining years of the project's lifetime, based on linear depreciation and the most practical strategies for ensuring an uninterrupted power supply and an energy demand balance based on hourly length [29]. All possible HRES plans are tested, and the workable configurations are then identified and ranked according to the design goals.

5.2. Simulation Analysis. The modelling system is primarily dependent on the designer's selection of components. HOMER is in response to the system's overall operations; as a result, the system generates large amounts of elements and develops in size. In this research, the HES must also be evaluated as the total sum of PV, WT, DG, battery, FC, and converter. The simulation study selects the most efficient dynamic planning and system design based on the electricity demand. HOMER even calculates the entire cost of a hybrid system, including the capital, replacement, operation and maintenance, and fuel costs, among other things.

5.3. Sensitivity Analysis. Sensitivity evaluation is a factor over which the manufacturer has no control. HOMER reintegrates the HES based on the manufacturer's specified sensitivity factor. The costs of a WT, battery, and generator fuel are all sensitivity considerations. The list of distinct HRES elements will be examined for improvement, from the lowest to the highest total system NPC. The system's result shows the best elements obtained by the least total system NPC thus attained. In the proposed model, HOMER Pro software analyzes the consumption of RESs in the studied area, as illustrated in Figure 5. PV, WT generator, FC, DG, electrolyzer, hydrogen storage tank, converter, and battery systems are part of the proposed HRES network. The suggested network comprises two types of load buses: AC and DC. The power is produced by an AC bus coupled to DG and WTs; however, energy is produced by a DC bus coupled to PV, battery, and FC systems. When the battery's excess power exceeds the load on the electrolyzer, the electrolyzer energizes and produces hydrogen (H_2), which is deposited in hydrogen tanks.

6. Results and Discussion

The system's primary goal has already been established: to optimize the cost and size of an off-grid HES for distributing the study region's essential energy demand. Depending on the information supplied, the proposed design is simulated with HOMER Pro software. After hourly simulation, alternative cost parameters and size configurations are obtained, as seen in Figure 10. Four different configurations are suggested, with the results of each configuration analyzed below.

6.1. Configuration 1: PV-WTG-DG-FC-BATT. In configuration 1, the distribution of energy sources for providing the necessary energy demand in the study region included PV, FC, DG, battery, and WT generators, as illustrated in Figure 10(a). The system's various ratings were 2.75 MW, 250 kW, 25 kW, 3200 numbers of 1 kWh, and 115 numbers of 10 kW, respectively, with an estimated energy demand of 5,965,198 kWh/yr.

6.2. Configuration 2: PV-WTG-DG-BATT without Fuel Cell. PV, DG, battery, and WTGs are all considered in configuration 2, as illustrated in Figure 10(b). The system sizes of considered PV, DG, battery, and WTGs were 2.75 MW, 25 kW, 3200 numbers of 1 kWh, and 115 numbers of 10 kW, with a total energy consumption 5,425,165 kWh/yr.

6.3. Configuration 3: PV-DG-FC-BATT without WTG. PV, DG, FC, and battery systems are all considered in configuration 3, as illustrated in Figure 10(c). The system sizes of PV, DG, FC, and battery systems were 2.75 MW, 25 kW, 250 kW, and 3200 numbers of 1 kWh correspondingly, with a total energy consumption 4,685,167 kWh/yr.

6.4. Configuration 4: PV-DG-BATT without WTG and Fuel Cell. In configuration 4, PV, DG, and battery systems are taken into account here, as shown in Figure 10(d). PV, DG, and battery system sizes were 2.75 MW, 25 kW, and 3200 numbers of 1 kWh, respectively, with an estimated energy demand of 3,455,324 kWh/yr.

6.5. Breakdown of Cost. The net cost estimation of all the components of configuration 1 is illustrated in Figure 11. The lead-acid battery has the greatest net cost of Rs. 1,014,869,656, while FC has the least net cost of Rs. 2,803,456.78. Figure 12 depicts various configurations' NPC, COE, and operational cost optimization findings.

6.6. Generation of Electricity per Year. Figure 13 depicts monthly energy production for HRES during the scheduled period. The annual energy produced by the WTs, PV system, DG, and FC is 1,919,480 kWh/yr, 4,845,216 kWh/yr, 90,343 kWh/yr, and 1,469,306 kWh/yr, correspondingly.

The modelling proposal developed as a result of this research facilitated the simulation of the performance of an HRES case study integrating PV, WT, FC, DG, and batteries in VIT, Vellore, respectively. With the RESs considered, the evaluation is to identify the optimal one out of four configurations. Iterative results of specific components are shown in Figure 14. The optimization has been acquired with configuration 1 with minimal operating cost.

Figure 15 depicts the randomly chosen seven-day energy production and consumption scenario during the HMG's one-year operational period. Figure 15 examines the load, battery, fuel cell, and PV power generation. Figure 16 depicts the energy used over the course of seven days by DC and AC loads separately. Figure 16 also shows the overall amount of

renewable energy that is obtained from the HMG. Table 1 shows the COE of the four scenarios that were analyzed and optimized in the HOMER system.

Figures 17 and 18 depict the output power of an inverter, rectifier, solar panel, and wind turbine at various hours of the day in relation to its capacity and generation over various months of the year. The microgrid's storage system, which consists of a fuel cell and a battery, is where excess solar and wind energy is stored. The battery has a responsibility throughout the year as a backup resource. In times of need and insufficient power, the battery produced electricity. Figure 17 shows the output of the inverter and rectifier with 2,664,657 kWh/yr and 226,705 kWh/yr. The losses for this inverter and the rectifier are 140,245 kWh/yr and 11,932 kWh/yr. Similarly, for the 24 hours in a day in the case studies of VIT and Vellore, respectively, Figure 18 illustrates the PV and WT power output year-round. In MG's storage system, which is made up of a fuel cell and a battery, the excess energy produced by solar and wind power is stored. Figure 18(a) makes it clear that the PV panel runs from 6 a.m. to 6 p.m. (during the day) at a levelized cost of Rs. 7.63/kWh while the WT operates continuously throughout the day (24 hours) at a levelized cost of Rs. 13.4/kWh.

6.7. Emissions Generated from the Proposed System. To achieve CO₂ emissions, no expenditures are taken into account in this analysis. Table 2 lists the harmful emissions produced by RESs in configuration 1, in which CO₂ emissions are the highest and particulate matter emissions are the lowest in the listed emissions.

7. Future Scope of the Research

Future SG implementation will require rectifying technological, financial, and environmental issues. One of the most crucial ones is offering a high level of protection in both grid-connected and islanded modes of operation. Intelligent coordination across the communication, control, and protection areas is required to develop hybrid AC/DC MGs as an integral component of SGs. It will be vital for these three fields to grow simultaneously in MGs.

7.1. Development of Communication Infrastructures. By enabling a two-way link between network components and the management unit, communication technologies are crucial to the operation of MGs. Home area networks (HANs), field area networks (FANs), and wide area networks (WANs) are the three basic clusters into which the communication networks in an MG can be divided. Using bidirectional communications between the customers' electrical equipment and smart metres, which typically have a bandwidth of between 10 and 100 kbps, HANs are widely used to provide customers with information about their electricity consumption. HANs can use various communication technologies, including Bluetooth, Zigbee, and Wi-Fi [32, 33]. The acquired data from smart metres must be sent to the control centre via HANs and FANs. Wi-Fi, WiMax,

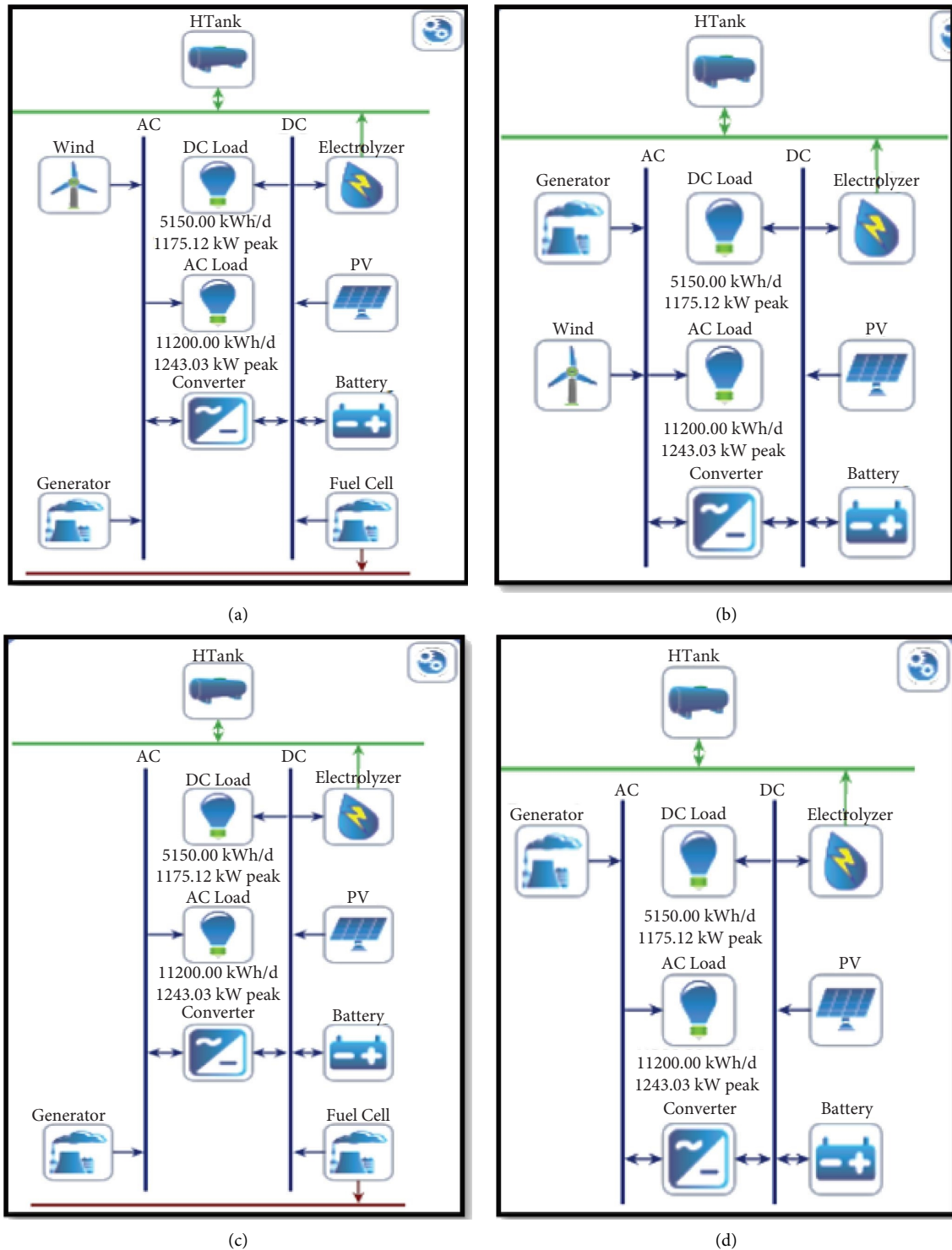


FIGURE 10: Proposed HRES. (a) Configuration 1. (b) Configuration 2. (c) Configuration 3. (d) Configuration 4.

radio frequency (RF), power line communication (PLC), general packet radio service (GPRS), and Enhanced Data Rates for GSM Evolution are among the communication technologies that can be used in FANs [34]. WANs are large-scale networks that enable two-way communication between MGs and the main grid. They can also be used as external networking devices to replenish information operators. The

most popular technology for these networks is WiMax because of its broad coverage [35].

7.2. Development of Integrated Control and Protection Strategy. Future hybrid AC/DC microgrids can effectively address the following issues by combining control and protection schemes: (a) self-healing, which refers to the

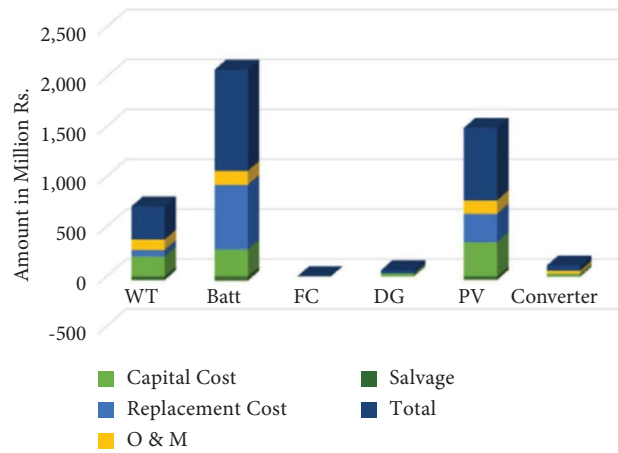


FIGURE 11: Net cost summary of the component.

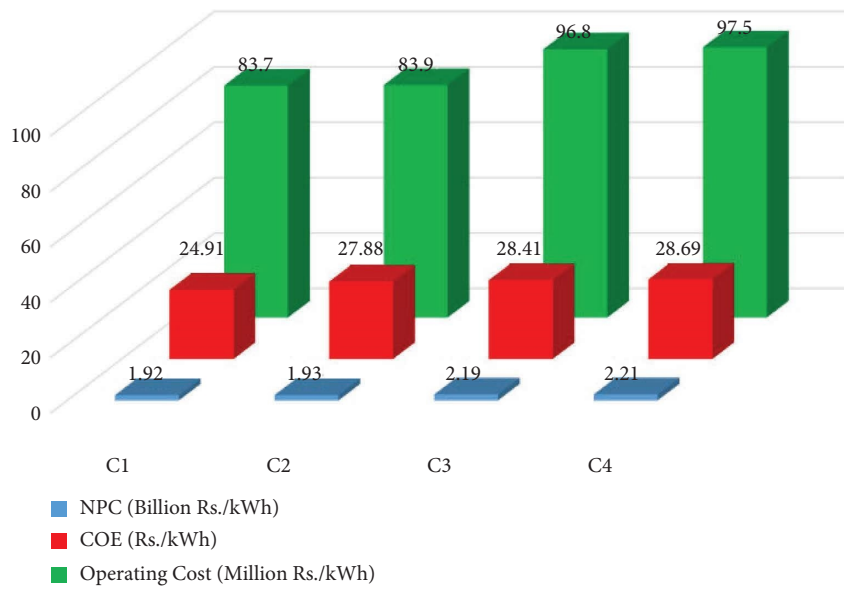


FIGURE 12: Comparison of different HRESs with operating cost, NPC, and COE.

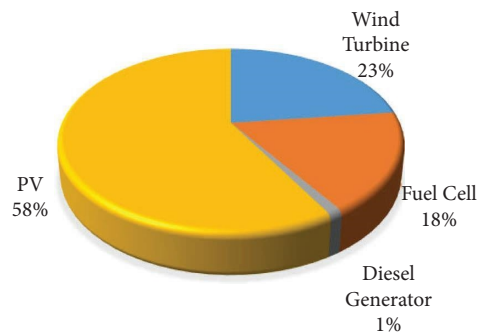


FIGURE 13: Monthly electrical generation during a year.

ability to quickly restore resilience of the power system in response to short-circuit conditions [36], (b) low-voltage ride through, which is defined as the ability of generators

to remain connected in brief periods of lower electric network voltage, and (c) driving current to zero before it reaches zero. Nevertheless, integration with

	PV (kW)	G10	FC (kW)	Gen25 (kW)	1kWh LA	Electrolyzer (kW)	HTank (kg)	Converter (kW)	NPC (₹)	COE (₹)	Operating cost (₹/yr)	Initial capital (₹)	Fuel cost (₹/yr)	O&M (₹/yr)
	5,450				98,040			1,243	₹3,358	₹43.43	₹141M	₹1,538	₹0.00	₹56.3M
	5,450				98,040		10.0	1,243	₹3,358	₹43.43	₹141M	₹1,538	₹0.00	₹56.3M
	5,450				98,040	10.0		1,243	₹3,358	₹43.46	₹141M	₹1,538	₹0.00	₹56.3M
	5,450				98,040	10.0	10.0	1,243	₹3,358	₹43.46	₹141M	₹1,538	₹0.00	₹56.3M
	4,945			25.0	86,580			1,220	₹3,178	₹41.15	₹139M	₹1,378	₹3.88M	₹50.5M
	4,945			25.0	86,580		10.0	1,220	₹3,178	₹41.15	₹139M	₹1,378	₹3.88M	₹50.5M
	4,945			25.0	86,580	10.0		1,220	₹3,178	₹41.19	₹139M	₹1,378	₹3.88M	₹50.5M
	4,945			25.0	86,580	10.0	10.0	1,220	₹3,188	₹41.19	₹139M	₹1,378	₹3.88M	₹50.5M
	4,068		250		49,450			1,441	₹2,218	₹28.69	₹97.5M	₹951M	₹93,058	₹35.2M
	4,068		250		49,450		10.0	1,441	₹2,218	₹28.69	₹97.5M	₹951M	₹93,058	₹35.2M
	4,068		250		49,450	10.0		1,441	₹2,218	₹28.73	₹97.5M	₹954M	₹93,058	₹35.2M
	4,068		250		49,450	10.0	10.0	1,441	₹2,218	₹28.73	₹97.5M	₹954M	₹93,058	₹35.2M
	3,874		250	25.0	50,500			1,413	₹2,198	₹28.37	₹96.7M	₹936M	₹3,51M	₹34.7M
	3,874		250	25.0	50,500		10.0	1,413	₹2,198	₹28.37	₹96.7M	₹936M	₹3,51M	₹34.7M
	3,874		250	25.0	50,500	10.0		1,413	₹2,198	₹28.40	₹96.8M	₹938M	₹3,51M	₹34.8M
	3,874		250	25.0	50,500	10.0	10.0	1,413	₹2,198	₹28.40	₹96.8M	₹938M	₹3,51M	₹34.8M
	3,874		250	25.0	50,500	10.0	10.0	1,413	₹2,198	₹28.41	₹96.8M	₹938M	₹3,51M	₹34.8M
	3,795	181			52,080			1,166	₹2,828	₹36.62	₹122M	₹1,258	₹0.00	₹47.1M
	3,795	181			52,080		10.0	1,166	₹2,828	₹36.63	₹122M	₹1,258	₹0.00	₹47.1M
	3,795	181			52,080	10.0		1,166	₹2,838	₹36.66	₹122M	₹1,258	₹0.00	₹47.1M
	3,795	181			52,080	10.0	10.0	1,166	₹2,838	₹36.66	₹122M	₹1,258	₹0.00	₹47.1M
	3,611	176		25.0	51,040			1,157	₹2,788	₹36.10	₹122M	₹1,218	₹3.80M	₹45.7M
	3,611	176		25.0	51,040		10.0	1,157	₹2,788	₹36.10	₹122M	₹1,218	₹3.80M	₹45.7M
	3,611	176		25.0	51,040	10.0		1,157	₹2,798	₹36.13	₹122M	₹1,218	₹3.80M	₹45.7M
	3,611	176		25.0	51,040	10.0	10.0	1,157	₹2,798	₹36.13	₹122M	₹1,218	₹3.80M	₹45.7M
	2,753	115	250	25.0	32,010	10.0	10.0	1,103	₹1,928	₹24.91	₹83.7M	₹838M	₹2,69M	₹31.7M
	2,611	117	250		34,530			1,159	₹1,938	₹24.99	₹83.9M	₹843M	₹4,244	₹32.2M

FIGURE 14: Optimization results using HOMER.

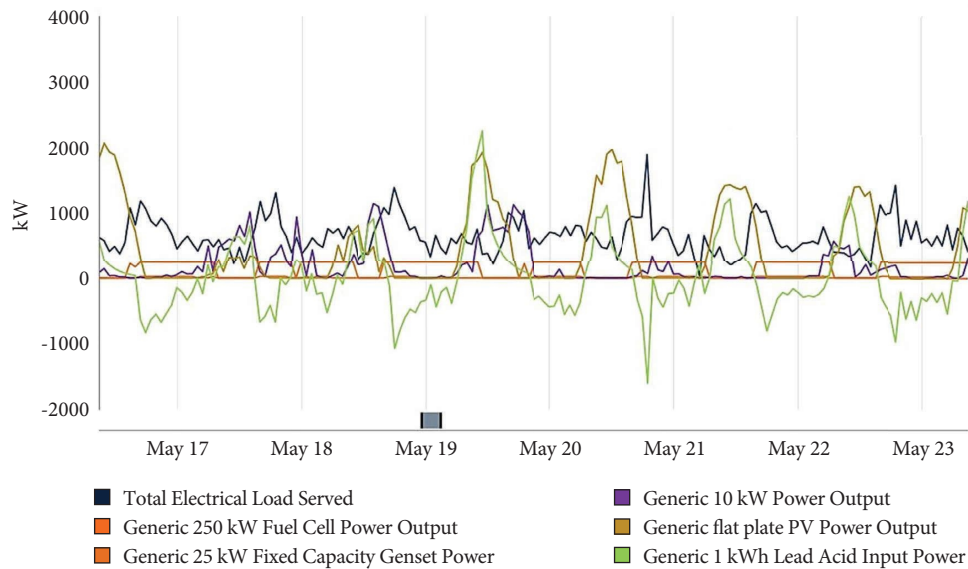


FIGURE 15: Hourly operation of electrical sources according to HOMER.

communication and information infrastructures is necessary for the formation of combined control and protection strategies.

7.3. Development of Smart Control and Protection Devices. In past years, solid state transformers (SSTs), one of the most innovative technologies, have received a lot of attention [37]. In addition to having the capacity to step up or down voltage

levels, SSTs, which are made up of high-power semiconductor components, high-frequency transformers, and control circuitry, can also offer the following benefits: power flow can be managed, AC and DC connections are available, short-circuit currents can be limited, and switching among MG operating modes is simple. Furthermore, employing SSTs in hybrid AC/DC MGs of the future requires additional economic and reliability evaluation.

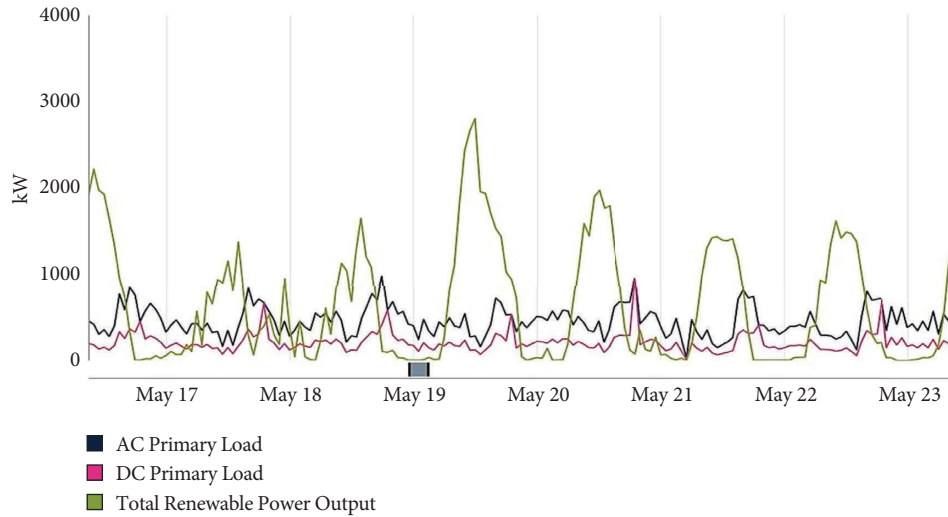


FIGURE 16: Hourly operation of both AC load and DC load according to HOMER.

TABLE 1: Hybrid configurations and COE.

Sl. No	Configuration	NPC (billion Rs/kWh)	Operating cost (million Rs/kWh)	COE (Rs/kWh)
1	PV-WTG-DG-FC-BATT	1.92	83.7	24.91
2	PV-WTG-DG-BATT	1.93	83.9	27.88
3	PV-DG-FC-BATT	2.19	96.8	28.41
4	PV-DG-BATT	2.21	97.5	28.69

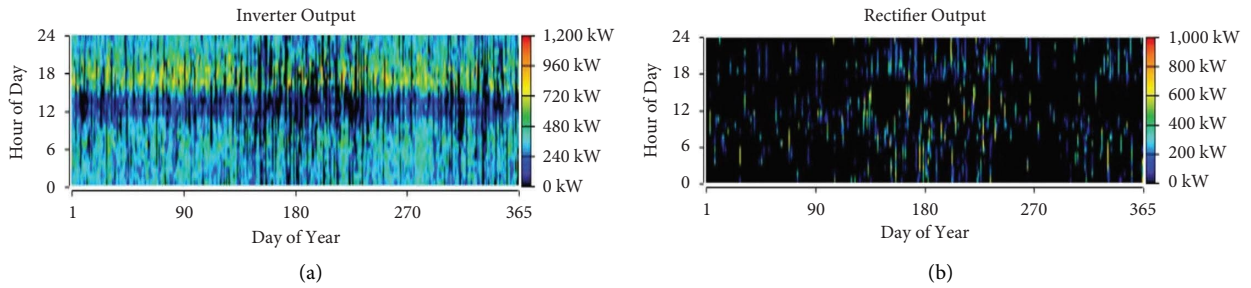


FIGURE 17: (a) Inverter output and (b) rectifier output.

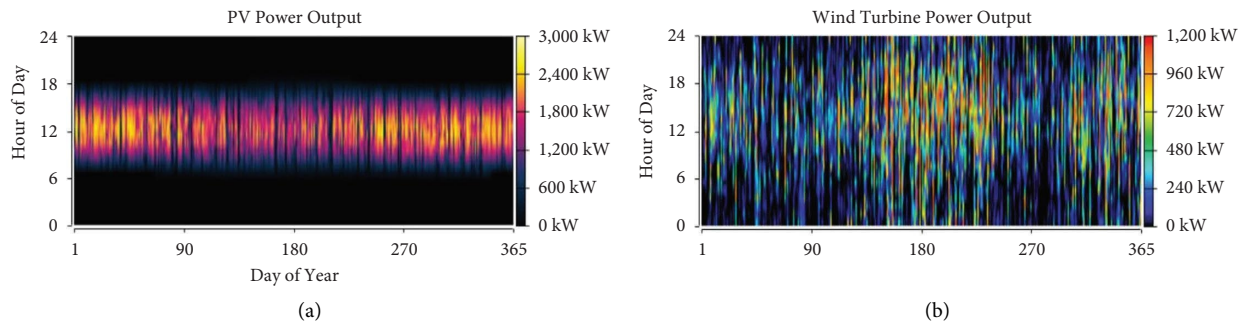


FIGURE 18: (a) PV output and (b) WT output.

TABLE 2: Total emissions generated by proposed system.

Contaminant	Amount (kg/yr)
CO ₂	671,106
Carbon monoxide	513
Unburned hydrocarbons	19.9
Particulate matter	2.71
Sulphur dioxide	177
Nitrogen oxides	431

8. Conclusion

According to techno-economic analyses conducted using HOMER and MATLAB along with FCS-MPC of an ILC to meet the electrical needs of VIT in Vellore, Tamil Nadu, a stand-alone HRES with configuration 1 is offered as the finest and most economically feasible system. The design of a system operating strategy considers several issues, including source allocation, economic comparisons, energy demand estimation, and system emissions. In addition, the HOMER Pro software was used to test four different HES configurations. Four configurations, namely, (1) PV-WTG-DG-FC-BATT, (2) PV-WTG-DG-BATT without fuel cell, (3) PV-DG-FC-BATT without WTG, and (4) PV-DG-BATT without WTG and fuel cell, were analyzed. Based on the total NPC and COE in the study region, these four configurations are investigated and evaluated. To begin, the four HRES combinations are assessed using HOMER. The first of these configurations yields the lowest NPC and COE of Rs. 1.92 billion and Rs. 24.91, respectively. In addition, CO₂ emissions are examined.

Data Availability

The data used to support the findings of this study are available from the corresponding author upon request.

Conflicts of Interest

The authors declare that they have no conflicts of interest.

Authors' Contributions

Vasantharaj Subramanian was responsible for investigation, methodology, and original draft preparation. Indragandhi Vairavasundaram was responsible for project administration, supervision, and validation. Belqasam Aljafari was responsible for formal analysis, software, resources, and review and editing.

Acknowledgments

The authors are thankful to the Deanship of Scientific Research at Najran University for funding this work under the Research Groups Funding Program (grant code: NU/RG/SERC/12/7).

References

[1] S. Vendoti, M. Muralidhar, and R. Kiranmayi, "Performance analysis of hybrid power system along with conventional

energy sources for sustainable development in rural areas," *International Journal of Recent Technology and Engineering*, vol. 8, no. 3, pp. 5971–5977, 2019.

- [2] S. Rajanna and R. P. Saini, "Employing demand side management for selection of suitable scenario-wise isolated integrated renewal energy models in an Indian remote rural area," *Renewable Energy*, vol. 99, pp. 1161–1180, 2016.
- [3] S. Vendoti, M. Muralidhar, and R. Kiranmayi, "Techno-economic analysis of off-grid solar/wind/biogas/biomass/fuel cell/battery system for electrification in a cluster of villages by HOMER software," *Environment, Development and Sustainability*, vol. 23, no. 1, pp. 351–372, 2021.
- [4] M. Zand, M. A. Nasab, P. Sanjeevikumar, P. K. Maroti, and J. B. Holm-Nielsen, "Energy management strategy for solid-state transformer-based solar charging station for electric vehicles in smart grids," *IET Renewable Power Generation*, vol. 14, no. 18, pp. 3843–3852, 2020.
- [5] M. Azimi Nasab, M. Zand, M. Eskandari, P. Sanjeevikumar, and P. Siano, "Optimal planning of electrical appliance of residential units in a smart home network using cloud services," *Smart Cities*, vol. 4, no. 3, pp. 1173–1195, 2021.
- [6] D. Xia, S. Ba, and A. Ahmadpour, "Non-intrusive load disaggregation of smart home appliances using the IPPO algorithm and FHM model," *Sustainable Cities and Society*, vol. 67, Article ID 102731, 2021.
- [7] M. A. Nasab, M. Zand, S. Padmanaban, M. S. Bhaskar, and J. M. Guerrero, "An efficient, robust optimization model for the unit commitment considering renewable uncertainty and pumped-storage hydropower," *Computers & Electrical Engineering*, vol. 100, Article ID 107846, 2022.
- [8] M. Azimi Nasab, M. Zand, S. Padmanaban, and B. Khan, "Simultaneous long-term planning of flexible electric vehicle photovoltaic charging stations in terms of load response and technical and economic indicators," *World Electric Vehicle Journal*, vol. 12, no. 4, p. 190, 2021.
- [9] O. Krishan and S. Suhag, "Grid-independent PV system hybridization with fuel cell-battery/supercapacitor: optimum sizing and comparative techno-economic analysis," *Sustainable Energy Technologies and Assessments*, vol. 37, Article ID 100625, 2020.
- [10] R. Bayindir, E. Hossain, E. Kabalci, and R. Perez, "A comprehensive study on microgrid technology," *International Journal of Renewable Energy Resources*, vol. 4, no. 4, pp. 1094–1107, 2014.
- [11] A. Rezvani and M. Gandomkar, "Simulation and control of intelligent photovoltaic system using new hybrid fuzzy-neural method," *Neural Computing & Applications*, vol. 28, no. 9, pp. 2501–2518, 2017.
- [12] M. Botzung, S. Chaudourne, O. Gillia et al., "Simulation and experimental validation of a hydrogen storage tank with metal hydrides," *International Journal of Hydrogen Energy*, vol. 33, no. 1, pp. 98–104, 2008.
- [13] Z. Liu, J. Zhao, and Z. Zou, "Impedance Modeling, dynamic Analysis and damping enhancement for DC Microgrid with multiple types of loads," *International Journal of Electrical Power & Energy Systems*, vol. 122, Article ID 106183, 2020.
- [14] Z. Liu, M. Su, Y. Sun, W. Yuan, H. Han, and J. Feng, "Existence and stability of equilibrium of DC microgrid with constant power loads," *IEEE Transactions on Power Systems*, vol. 33, no. 6, pp. 6999–7010, 2018.
- [15] X. Kong, X. Liu, L. Ma, and K. Y. Lee, "Hierarchical distributed model predictive control of standalone wind/solar/battery power system," *IEEE Transactions on Systems, Man, and Cybernetics: Systems*, vol. 49, no. 8, pp. 1570–1581, 2019.

- [16] M. Mehreganfar, M. H. Saeedinia, S. A. Davari, C. Garcia, and J. Rodriguez, "Sensorless predictive control of AFE rectifier with robust adaptive inductance estimation," *IEEE Transactions on Industrial Informatics*, vol. 15, no. 6, pp. 3420–3431, 2019.
- [17] F. Salem and M. I. Mosaad, "A comparison between MPC and optimal PID controllers: case studies," in *Proceedings of the Michael Faraday IET International Summit*, pp. 59–65, Kolkata, India, September, 2015.
- [18] Y. W. Shen, J. R. Yuan, F. F. Shen, J. Z. Xu, C. K. Li, and D. Wang, "Finite control set model predictive control for complex energy system with large-scale wind power," *Complexity*, vol. 2019, Article ID 4358958, 13 pages, 2019.
- [19] V. Suresh, M. Muralidhar, and R. Kiranmayi, "Modelling and optimization of an off-grid hybrid renewable energy system for electrification in a rural-areas," *Energy Reports*, vol. 6, pp. 594–604, 2020.
- [20] J. Kitson, S. J. Williamson, P. Harper et al., "A photovoltaic panel modelling method for flexible implementation in Matlab/Simulink using datasheet quantities," in *Proceedings of the 2017 IEEE 26th International Symposium on Industrial Electronics (ISIE)*, pp. 946–951, Edinburgh, UK, June, 2017.
- [21] J. Kitson, S. J. Williamson, P. W. Harper et al., "Modelling of an expandable, reconfigurable, renewable DC microgrid for off-grid communities," *Energy*, vol. 160, pp. 142–153, 2018.
- [22] A. B. Kanase-Patil, R. Saini, and M. Sharma, "Sizing of integrated renewable energy system based on load profiles and reliability index for the state of Uttarakhand in India," *Renewable Energy*, vol. 36, no. 11, pp. 2809–2821, 2011.
- [23] V. Thapar, G. Agnihotri, and V. K. Sethi, "Critical analysis of methods for mathematical modelling of wind turbines," *Renewable Energy*, vol. 36, no. 11, pp. 3166–3177, 2011.
- [24] R. S. Garcia and D. Weisser, "A wind-diesel system with hydrogen storage: joint optimisation of design and dispatch," *Renewable Energy*, vol. 31, no. 14, pp. 2296–2320, 2006.
- [25] M. J. Khan and M. T. Iqbal, "Dynamic modeling and simulation of a small wind-fuel cell hybrid energy system," *Renewable Energy*, vol. 30, no. 3, pp. 421–439, 2005.
- [26] S. Vendoti, M. Muralidhar, and R. Kiranmayi, "Design and analysis of solar PV-fuel cell-battery based hybrid renewable energy system (HRES) for off-grid electrification in rural areas," *i-Manager's Journal on Instrumentation & Control Engineering*, vol. 6, no. 3, 2018.
- [27] T. F. El-Shatter, M. N. Eskander, and M. T. El-Hagry, "Energy flow and management of a hybrid wind/PV/fuel cell generation system," *Energy Conversion and Management*, vol. 47, no. 9–10, pp. 1264–1280, 2006.
- [28] H. U. R. Habib, S. Wang, M. R. Elkadeem, and M. F. Elmorshedy, "Design optimization and model predictive control of a standalone hybrid renewable energy system: a case study on a small residential load in Pakistan," *IEEE Access*, vol. 7, pp. 117369–117390, 2019.
- [29] E. Diemuodeke, A. Addo, C. Oko, Y. Mulugetta, and M. Ojapah, "Optimal mapping of hybrid renewable energy systems for locations using multi-criteria decision-making algorithm," *Renewable Energy*, vol. 134, pp. 461–477, 2019.
- [30] O. Krishan and S. Suhag, "Techno-economic analysis of a hybrid renewable energy system for an energy poor rural community," *Journal of Energy Storage*, vol. 23, pp. 305–319, 2019.
- [31] C. Bastholm and F. Fiedler, "Techno-economic study of the impact of blackouts on the viability of connecting an off-grid PV-diesel hybrid system in Tanzania to the national power grid," *Energy Conversion and Management*, vol. 171, pp. 647–658, 2018.
- [32] B. Al-Omar and A. Al-Ali, "Role of information and communication technologies in the smart grid," *Journal of Emerging Trends in Computing and Information Sciences*, vol. 3, no. 5, pp. 707–716, 2012.
- [33] L. K. Siow, P. L. So, H. B. Gooi, F. L. Luo, C. J. Gajanayake, and Q. N. Vo, "Wi-Fi based server in microgrid energy management system," in *Proceedings of the TENCON 2009 – 2009 IEEE Region 10 Conference*, pp. 1–5, Singapore, January, 2009.
- [34] A. P. Sakis Meliopoulos, G. Cokkinides, R. Huang et al., "Smart grid technologies for autonomous operation and control," *IEEE Transactions on Smart Grid*, vol. 2, no. 1, pp. 1–10, 2011.
- [35] A. Gopalakrishnan and A. C. Biswal, "Applications of emerging communication trends in automation," in *Proceedings of the IEEE 6th International Conference on Power Systems (ICPS)*, pp. 2–7, New Delhi, India, March, 2016.
- [36] S. Beheshtaein, M. Savaghebi, J. C. Vasquez, and J. M. Guerrero, "Protection of AC and DC microgrids: challenges, solutions and future trends," in *Proceedings of the IECON 2015 – 41st Annual Conference of the IEEE Industrial Electronics Society*, pp. 5253–5260, Yokohama, Japan, November, 2015.
- [37] S. A. Hosseini, H. A. Abyaneh, S. H. H. Sadeghi, F. Razavi, and A. Nasiri, "An overview of microgrid protection methods and the factors involved," *Renewable and Sustainable Energy Reviews*, vol. 64, pp. 174–186, 2016.